# SILICON NITRIDE-ON-SILICON BAR RESONATOR USING INTERNAL ELECTROSTATIC TRANSDUCTION

Sunil A. Bhave and Roger T. Howe
Berkeley Sensor & Actuator Center, 497 Cory Hall, University of California, Berkeley, CA 94720, USA

## ABSTRACT

This paper demonstrates an electrostatic transducer for lateral-mode bar resonators in which a high dielectric constant (high-κ) thin film is sandwiched between polysilicon electrodes and the top surface of the resonator. This *internal electrostatic transducer* has several advantages over both air-gap electrostatic and piezoelectric transduction, including lower motional impedance ($R_x$), compatibility with advanced scaled CMOS device technology, and extended dynamic range. The resonators are fabricated on 4 μm thick heavily-doped SOI wafers with 200 nm thick silicon nitride film as the dielectric transducer. Using this configuration, we have demonstrated a 121 MHz silicon nitride-on-silicon lateral-mode bar resonator with a quality factor ($Q$) of 2,100 in air and motional impedance of 9 kΩ.

**Keywords:** Resonator, RF MEMS, Electrostatic transducer, Silicon Nitride

## INTRODUCTION

Recent demand in single-chip, multi-standard wireless transceivers has focused research efforts towards developing on-chip, high-$Q$ MEMS resonators capable of substituting existing off-chip SAW and ceramic resonator technologies. FBARs (Film bulk acoustic resonators) have proven themselves as a valid solution to replace conventional RF filters, demonstrating relatively high $Q$ and small motional impedances. However, the resonant frequency of these devices is set by the piezoelectric film thickness. This constitutes a major challenge to manufacturing multi-frequency FBARs on the same chip as each desired frequency will need a separate deposition and etch step.

Unlike FBARs, the resonant frequency of lateral bulk acoustic resonators is defined by lithography dimensions. A single-mask can include multi-frequency filters, oscillators and mixers. However, air-gap lateral bulk acoustic resonators have a relatively large motional impedance $R_x$ due to reduced transducer area [1] and inefficient electrostatic transduction (compared to lateral $d_{31}$ piezoelectric transduction [2,3]). By increasing the transducer area, new designs such as coupled resonator arrays [4], bulk annular rings [5] and ultra-wide silicon bars [6] have reduced $R_x$. However, to reach motional impedances on the order of 50 Ω, (assuming 50 nm air-gaps) we would need a coupled array of 100 resonators, a 400μm diameter ring resonator or a 2 mm wide silicon bar. The signal routing challenges for these devices will be daunting at GHz frequencies and the chip area occupied by such a resonator will be larger than an FBAR.

Internal electrostatic transduction enhances both the force density of the actuator as well as the sense capacitance, thereby reducing the motional impedance of the resonator by $\kappa^2$. We previously proposed and experimentally verified internal electrostatic transduction using an aluminum nitride FBAR resonator in non-linear electrostatic mode [7]. In this paper, we demonstrate a 121 MHz 3rd harmonic lateral bar resonator with internal electrostatic actuation and sensing of the mechanical motion, by depositing silicon nitride (κ ~ 9) on the top surface of a silicon bar.

## LATERAL MODE BAR RESONATOR

Figure 1 shows a schematic diagram of the two-port silicon lateral bar resonator presented in this paper. The resonator is identical to the piezo-on-silicon resonator [2] except we used silicon nitride instead of zinc oxide and polysilicon electrodes instead of aluminum electrodes.

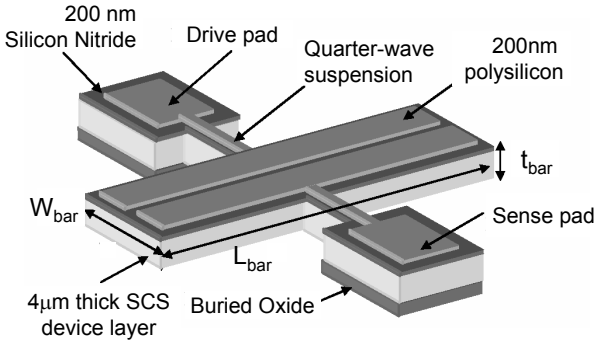


***Figure 1.*** *3D schematic of the lateral-mode bar resonator with 200 nm silicon nitride internal electrostatic transducer.*

The natural frequencies and motional impedance of the length extensional modes of the bar are given by [1,2,8]:

$$\omega_n = \frac{n\pi}{L_{bar}}\left(\sqrt{\frac{E}{\rho}}\right)_{Si} \; ; \; R_x = \frac{n\pi}{4}\cdot\frac{\sqrt{E\cdot\rho}}{Q}\cdot\frac{W_{bar}\cdot t_{bar}}{\eta^2}$$

where $n$ is the mode number ($n$ = 1,3,…), $L_{bar}$ , $W_{bar}$ and $t_{bar}$ are the length, width and thickness of the bar resonator, $\rho$ and $E$ are the density and Young's modulus of silicon and $\eta$ is the electromechanical coupling coefficient, which depends on the transduction scheme.

## INTERNAL ELECTROSTATIC TRANSDUCTION

Actuation and sensing of condenser microphone diaphragms [9] and audio-frequency cantilever beams [10] has been previously demonstrated by embedding silicon nitride dielectric capacitors in silicon bending-mode resonators. Both devices made use of Poisson's ratio ($\nu_{SiN}$) to convert applied strain normal to the beam's length, into strain along the beam, which coupled to the fundamental bending mode. The approach was deemed inefficient because air-gap electrostatic transduction provided larger displacement, the preferred performance metric at that time.

Bulk-mode resonators have significantly different design requirements compared to flexural resonators. With mechanical spring stiffness > 500 kN/m at 1 GHz, these resonators have displacements on the order of few hundred picometers. We can enhance the transduction efficiency and reduce the motional impedance of lateral-mode bar resonators by filling the air-gaps with a high-κ dielectric material. However, it is difficult to fabricate and fill a 4μm : 50nm (80:1) aspect ratio transducer gap with conformal high-κ dielectric using conventional micromachining technology (modern atomic layer deposition techniques can achieve dielectric thin films with conformality over high aspect ratio gaps [11]). Instead we deposit a thin silicon nitride layer on the top surface of the bar resonator.

When we apply a DC+AC electric field across the silicon nitride thin film, the compressive stress on the silicon nitride in the transverse direction is accompanied by a lateral stress along the length. Since the silicon nitride layer is structurally integrated with the silicon bar, the lateral stress is transferred from the dielectric film to the silicon resonator layer (Figure 2). This generates a lateral drive force on the resonator:

$$f_{drive} = \nu_{SiN} \cdot V_{DC} \cdot \frac{\varepsilon_0 \cdot \kappa_{SiN} \cdot A_{electrode}}{t_{SiN}^2} \cdot v_{ac}$$

and displacement at fundamental resonance:

$$x = \frac{f_{drive}}{K_{lateral}} \cdot Q = f_{drive} \cdot \frac{4 \cdot L_{bar}}{\pi^2 \cdot E_{Si} \cdot W_{bar} \cdot t_{bar}} \cdot Q$$

As the resonator vibrates, the top layer is harmonically stretched and compressed. This causes a fluctuation in both area and thickness of the silicon nitride thin film (Figure 3). When a DC voltage is applied between the sense polysilicon electrode and the resonator, the (re)charging of the capacitor yields a motional current:

$$i_{sense} = \nu_{SiN} \cdot V_{DC} \cdot \frac{\varepsilon_0 \cdot \kappa_{SiN} \cdot A_{electrode}}{t_{SiN}^2} \cdot \omega_0 \cdot x$$

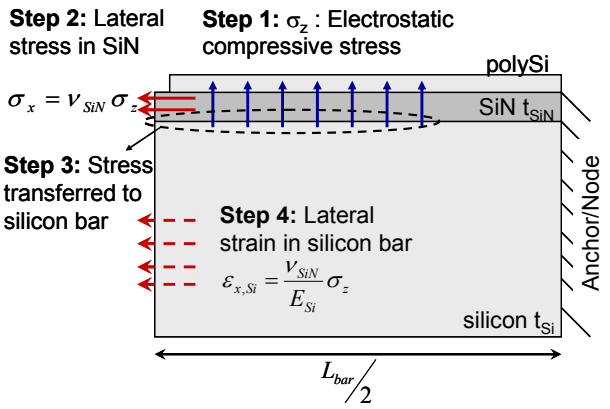


*Figure 2. 2D cross-section schematic of the conversion of transverse electrostatic stress in the silicon nitride thin film to lateral strain in the lateral-mode bar resonator. The approximation holds true for resonators of short length and medium thickness. For long lengths or very thin beams, the strain couples into the bending mode [10] instead of the lateral bulk acoustic mode of the beam. Half the bar length is illustrated for simplicity; the effect is symmetric about the anchor. The lateral strain along the resonator width is not shown.*

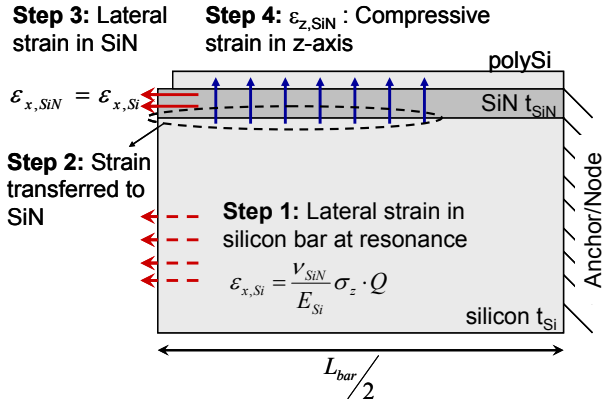


*Figure 3. 2D cross-section schematic of the conversion of lateral strain in the silicon bar resonator into lateral and transverse strain in the silicon nitride thin film.*

For the length symmetric electrode topology of these resonators, both the drive and sense electromechanical coupling coefficient is:

$$\eta = \alpha \cdot \nu_{SiN} \cdot V_{DC} \cdot \frac{\varepsilon_0 \cdot \kappa_{SiN} \cdot A_{electrode}}{t_{SiN}^2}$$

where α is the correction factor related to the mode-shape of the resonator and the Young's modulus of the silicon nitride thin film.

The motional impedance of lateral bar resonator is:

$$R_{x,n} = \frac{n\pi\sqrt{E \cdot \rho}}{4Q} \cdot \frac{W_{bar} \cdot t_{bar} \cdot t_{SiN}^4}{\alpha^2 \cdot V_{DC}^2 \cdot \nu_{SiN}^2 \cdot \varepsilon_0^2 \cdot \kappa_{SiN}^2 \cdot A_{electrode}^2}$$

The efficiency of internal electrostatic transduction can be increased by decreasing the thickness of the dielectric film, and by using a dielectric film with high values for Poisson's ratio and dielectric constant. In addition, reducing the thickness of the silicon resonator will allow efficient transfer of the lateral stress into the lateral bulk acoustic modes of the resonator. However, as the bar thickness reduces, the lateral stress will couple into the bending mode of the resonator.

## FABRICATION PROCESS

The resonators are fabricated in a 3-mask SOI process (Figure 4) and follow almost the same steps as reported in [2]. We start with a p-type low-resistivity SOI wafer with a 4 μm device layer and deposit 200 nm of stress-free silicon nitride thin film (LSN). The silicon nitride is patterned to open contact holes to ground (or DC bias) the silicon resonator. Then we deposit and anneal 200 nm of p-type heavily-doped polysilicon. The polysilicon is patterned to define the drive and sense electrodes, interconnect and the ground-signal-ground (GSG) pads. This is followed by a deep reactive ion etch (DRIE) step to define the resonator into the silicon device layer. Finally, we release the resonator in HF by a timed-etch of the buried oxide followed by critical point drying.

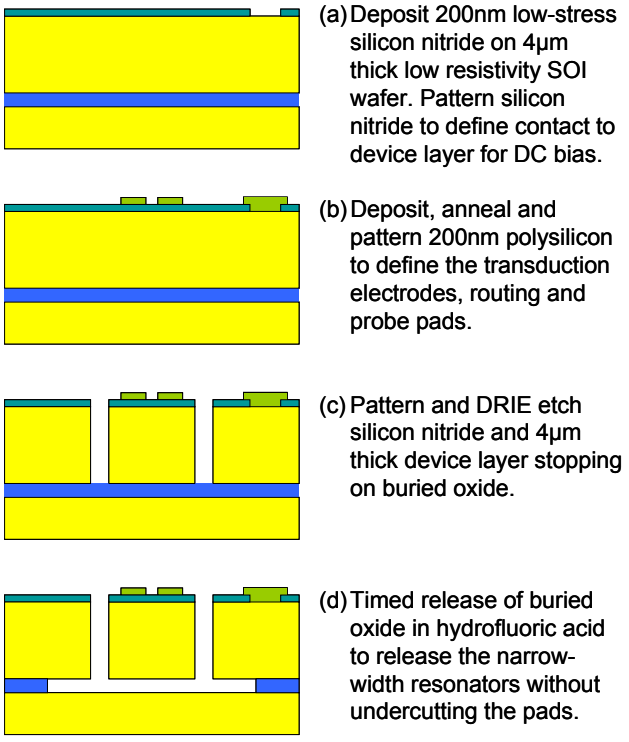


***Figure 4.*** *Fabrication process-flow for the silicon nitride-on-silicon lateral-mode bar resonators, adapted from [2]. A low resistivity device layer SOI wafer was used to prevent the electrical resistance from reducing the Q of the resonator.*

## EXPERIMENTAL RESULTS

The fabricated resonators were tested in air at room temperature on a Cascade Microtech microwave probe station with GSG probes and semi-rigid SMA cables. The resonator was grounded and a DC bias was applied to both the drive and sense electrodes using bias-Ts from MiniCircuits. Transmission measurements were performed using an Agilent 8753ES Network Analyzer and the quality factor and insertion loss were extracted from the measured data. The motional impedance of the resonator was extracted from the insertion loss data after adjusting for the attenuation losses at the drive pad ($C_{pad}$~ 3 pF).

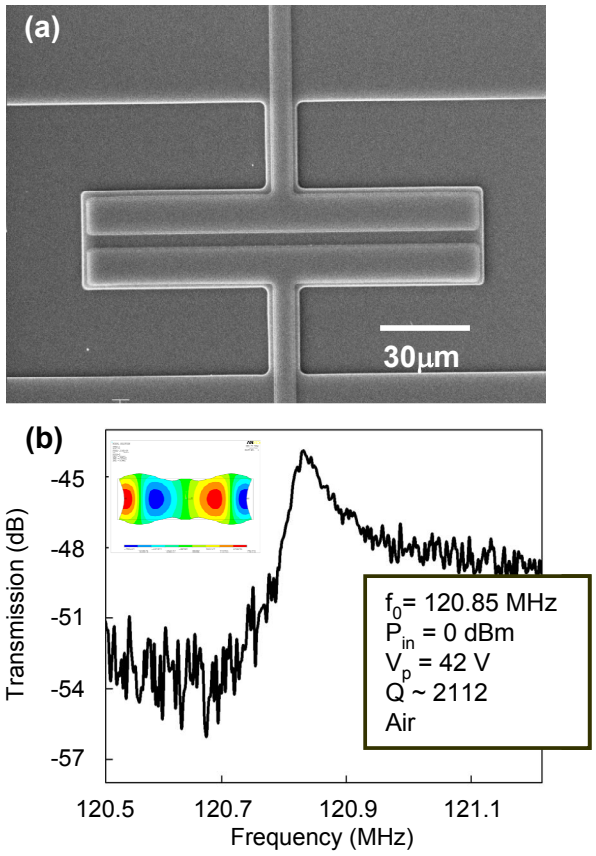


***Figure 5.*** *(a) SEM of a 100μm x 30μm silicon nitride-on-silicon lateral bar resonator. (b) Measured transmission of the 3rd harmonic mode of the resonator in air at 120.8 MHz. Inset shows the modal analysis of the resonator in ANSYS.*

We tested a 100μm long by 30μm wide bar resonator using a two port transmission measurement. The fundamental resonant frequency of 42 MHz could not be detected because the resonator has very low *Q* in air. However, air damping does not affect the quality factor of resonators above 100 MHz as the mechanical motion becomes comparable to the mean free path of air and we measured the 3rd harmonic mode at 121 MHz with a *Q* of 2,100 in air (Figure 5). The calculated motional

impedance of the resonator $R_x$ = 8.2 kΩ is very close to the measured motional impedance of 9 kΩ. Note that the enhancement in the motional impedance due to internal electrostatic transduction is limited because $\kappa_{SiN}$ is only about 9 and by the fact that the lateral mode is excited through Poisson coupling which causes $1/\nu_{SiN}^2 \sim 13\times$ increase in the motional impedance. Table 1 summarizes the $Q$ and insertion loss for silicon nitride-on-silicon resonators of different lengths and widths.

***Table 1.*** *Quality factor and Insertion Loss (I.L.) measurements in air for the fundamental and 3rd harmonic modes of silicon nitride-on-silicon lateral-mode bar resonators.*

| Size Length x Width (μm x μm) | Mode | Freq. (MHz) | *Q* (Air) | I.L. (dB) |
|---|---|---|---|---|
| 140 x 30 | 1 | 28 | - | - |
| 140 x 30 | 3 | 87 | 814 | -50 |
| 100 x 30 | 1 | 42 | - | -52 |
| 100 x 30 | 3 | 121 | 2112 | -45 |
| 60 x 20 | 1 | 68 | - | -44 |
| 60 x 20 | 3 | 203 | 1484 | -42 |

## CONCLUSIONS

High-κ dielectric materials like $TiO_2$ (κ = 80) and $HfO_2$ (κ = 25) are CMOS qualified, are readily available in state-of-the-art CMOS foundries and can be deposited conformally using atomic layer deposition. This will enable us to fill the narrow trenches of air-gap electrostatically transduced bar resonators with high-κ transducing dielectric, without reducing the electromechanical coupling efficiency due to Poisson's effect. The most appealing benefit in terms of manufacturing is because there are no air-gaps, the fabrication yield of these resonators is significantly higher than air-gap resonators.

We have demonstrated internal electrostatic transduction as an attractive alternative to air-gap electrostatic and piezoelectric transduction for bulk-mode MEMS resonators. By depositing the silicon nitride thin film on the top surface of the silicon bar resonator, the electromechanical coupling efficiency improved by $\kappa_{SiN}^2 \cdot \nu_{SiN}^2 \sim 6\times$ over air-gap electrostatic transduction. The low measured $Q$ of 2,100 (compared to air-gap resonators [1,5,6]) of the silicon nitride-on-silicon bar resonators suggests that more research is needed on the material losses of high-κ dielectrics and precautions need to be taken while choosing the right combination of dielectric and resonator materials. However, the 121 MHz silicon nitride-on-silicon lateral bar resonator demonstrates that internal electrostatic transduction is a promising approach for low-impedance integrated resonators.

## ACKNOWLEDGMENTS

The authors wish to thank Dr. Dan Radack and the DARPA NMASP program, whose generous grant (#N66001-00-1-8955) has made this research possible. We would also like to thank Sia Parsa, Hengky Chandrahalim, Shankar Radhakrishnan, Dong Yan, UC Berkeley Microlab and Cornell Nanofabrication Facility for resonator fabrication and Cornell Center for Nanoscale Systems for access to the microwave probe station.

## REFERENCES

[1] T. Mattila, *et al*, "Micromechanical Bulk Acoustic Wave Resonator," *Ultrasonics Symposium,* 2002, pp. 945-948.

[2] S. Humad, *et al*, "High Frequency Micromechanical Piezo-on-Silicon Block Resonators," *IEDM 2003*, pp. 957-960.

[3] G. Piazza, *et al*, "Low Motional Resistance Ring-Shaped Contour-Mode Aluminum Nitride Piezoelectric Micromechanical Resonators for UHF Applications," *MEMS 2005*, pp. 20-23.

[4] M. Demirci, *et al*, "Mechanically Corner-Coupled Square Microresonator Array for Reduced Series Motional Resistance," *Transducers 2003*, pp. 955-958.

[5] S. -S. Li, *et al*, "Micromechanical 'Hollow-Disk' Ring Resonators," *MEMS 2004*, pp. 821-824.

[6] S. Pourkamali, *et al*, "Vertical Capacitive SiBARs," *MEMS 2005*, pp. 211-214.

[7] S. A. Bhave and R. T. Howe, "Internal Electrostatic Transduction for Bulk-Mode MEMS Resonators," *Hilton Head 2004*, pp. 59-60.

[8] R. A. Johnson, "Mechanical Filters in Electronics," New York, NY, Wiley, 1983.

[9] F. A. Fischer, "Fundamentals of Electroacoustics," London, UK, Interscience Publishers, 1955.

[10] S. Bouwstra, *et al*, "Excitation and Detection of Vibrations of Micromechanical Structures using a Dielectric Thin Film," *Sensors and Actuators*, 17 (1989), pp. 219-223.

[11] R. G. Gordon, *et al*., "A kinetic model for step coverage by atomic-layer deposition in narrow trenches," *Chemical Vapor Deposition*, 9 (2003), pp. 73-78.